NPS 67-80-018

LEVEL II

(2)

NAVAL POSTGRADUATE SCHOOL
Monterey, California

AD A100110

JUN 1 3 1981

A

THESIS

FLOW CONTROL ABOUT AN
AIRBORNE LASER TURRET

by

James Robert Schonberger

December, 1980

Thesis Advisor: A. E. Fuhs

Approved for public release; distribution unlimited

Prepared for: Captain Richard deJonckheere, USAF
Air Force Weapons Laboratory
AFWL/ARLB
Kirtland AFB
Albuquerque, New Mexico

DTIC FILE COPY

NAVAL POSTGRADUATE SCHOOL
Monterey, California

Rear Admiral J. J. Ekelund
Superintendent

David Schrady
Acting Provost

This thesis prepared in conjunction with research supported in part by the Air Force Weapons Laboratory.

Reproduction of all or part of this report is authorized.

Released as a
Technical Report by:

William M. Tolles

W. M. Tolles
Dean of Research

UNCLASSIFIED

SECURITY CLASSIFICATION OF THIS PAGE (When Data Entered)

REPORT DOCUMENTATION PAGE

READ INSTRUCTIONS BEFORE COMPLETING FORM

1. REPORT NUMBER: NPS 67-80-018

2. GOVT ACCESSION NO.: AD-A100 110

3. RECIPIENT'S CATALOG NUMBER:

4. TITLE (and Subtitle): Flow Control About an Airborne Laser Turret

5. TYPE OF REPORT & PERIOD COVERED: Master's Thesis; December, 1980

6. PERFORMING ORG. REPORT NUMBER:

7. AUTHOR(s): James Robert Schonberger

8. CONTRACT OR GRANT NUMBER(s):

9. PERFORMING ORGANIZATION NAME AND ADDRESS: Naval Postgraduate School, Monterey, California 93940

10. PROGRAM ELEMENT, PROJECT, TASK AREA & WORK UNIT NUMBERS:

11. CONTROLLING OFFICE NAME AND ADDRESS: Naval Postgraduate School, Monterey, California 93940

12. REPORT DATE: December, 1980

13. NUMBER OF PAGES: 63

14. MONITORING AGENCY NAME & ADDRESS (if different from Controlling Office): Air Force Weapons Laboratory, AFWL/ARLB, Kirtland AFB, Albuquerque, New Mexico

15. SECURITY CLASS. (of this report): UNCLASSIFIED

15a. DECLASSIFICATION/DOWNGRADING SCHEDULE:

16. DISTRIBUTION STATEMENT (of this Report): Approved for public release; distribution unlimited

17. DISTRIBUTION STATEMENT (of the abstract entered in Block 20, if different from Report):

18. SUPPLEMENTARY NOTES:

19. KEY WORDS (Continue on reverse side if necessary and identify by block number):

AIRFLOW CONTROL
LASER
LASER PROPAGATION
LASER JITTER
LASER TURRET

20. ABSTRACT (Continue on reverse side if necessary and identify by block number)

A high-energy laser system inflicts damage on a target by radiating large amounts of thermal energy onto a small area. Airflow about the laser turret housed on top of an aircraft is unsteady, and causes problems in beam control. These problems are jitter, which is vibration of the laser beam, and optical path distortions.

The theory of flow around a cylinder and around a sphere was examined, and several airflow control techniques were investigated as possible means

DD FORM 1 JAN 73 1473 EDITION OF 1 NOV 65 IS OBSOLETE
S/N 0102-014-6601

UNCLASSIFIED

SECURITY CLASSIFICATION OF THIS PAGE (When Data Entered)

Block 20 (cot'd.)

of suppressing the unsteadiness of the flow. A fairing and turret-base suction apparatus was selected, and was experimentally tested in a wind tunnel.

During the course of the experiment, several parameters were varied, as follows: blower flow rate, spacing between turret and fairing nose piece, and flow rate in five separate ducts. Results of the tests utilizing the tapered symmetric nose piece indicate that the fairing and base-suction technique eliminates the unsteadiness. Further research and testing are required to develop this technique for actual use on aircraft.

Approved for public release; distribution unlimited

Flow Control About an Airborne Laser Turret

by

James Robert Schonberger
Lieutenant, United States Navy
B.A., North Dakota State University at Fargo, 1973

Submitted in partial fulfillment of the
requirements for the degree of

MASTER OF SCIENCE IN ENGINEERING SCIENCE

from the

NAVAL POSTGRADUATE SCHOOL
December 1980

Author: James R Schonberger

Approved by: Allen E Fuhs
Thesis Advisor

T. H. Gawain
Second Reader

M. F. Platzer
Chairman, ~~Department~~ of Aeronautics

William M. Tolles
Dean of Science and Engineering

ABSTRACT

A high-energy laser system inflicts damage on a target by radiating large amounts of thermal energy onto a small area. Airflow about the laser turret housed on top of an aircraft is unsteady, and causes problems in beam control. These problems are jitter, which is vibration of the laser beam, and optical path distortions.

The theory of flow around a cylinder and around a sphere was examined, and several airflow control techniques were investigated as possible means of suppressing the unsteadiness of the flow. A fairing and turret-base suction apparatus was selected, and was experimentally tested in a wind tunnel.

During the course of the experiment, several parameters were varied, as follows: blower flow rate, spacing between turret and fairing nose piece, and flow rate in five separate ducts. Results of the tests utilizing the tapered symmetric nose piece indicate that the fairing and base-suction technique eliminates the unsteadiness. Further research and testing are required to develop this technique for actual use on aircraft.

COMMENT CONCERNING JOINT RESEARCH EFFORT

This thesis and *Control of Airflow About a High Energy Laser Turret*, a thesis by LT Alan Mandigo [1], were the result of a joint research project. The flow control concept, experimental apparatus with the exception of the fairing nose piece, and instrumentation were common to both theses. The experimental results in this thesis are based on the tapered symmetric nose piece. The results in Ref. 1 are for the uniform conformal nose piece.

TABLE OF CONTENTS

I. INTRODUCTION 12

A. BACKGROUND 12

B. THESIS OBJECTIVE 13

II. THEORETICAL FLOW OF INVISCID FLUIDS AND VISCOUS EFFECTS 14

A. POTENTIAL FLOW ABOUT A CYLINDER 14

B. POTENTIAL FLOW ABOUT A SPHERE 16

C. VISCOUS EFFECTS AND FLOW SEPARATION 16

III. FLOW CONTROL 19

A. SURVEY OF VARIOUS PROPOSED METHODS 19

1. Off-Turret Control 19

2. Slot Blowing 19

3. Base Suction with Trapped Vortices 19

4. Base Suction 20

B. TEST METHOD 20

IV. EXPERIMENTAL APPARATUS 21

A. WIND TUNNEL 21

B. BLOWER SPECIFICATIONS 21

C. FAIRING DESIGN 22

D. FAIRING NOSE PIECE DESIGN 23

E. TURRET DESIGN 23

F. MODEL INSTALLATION 23

V. INSTRUMENTATION 24

A. PRESSURE TAPS 24

B. WIND TUNNEL DATA ACQUISITION SYSTEM 24

C. TUFTS 25

VI. EXPERIMENTS AND EXPERIMENTAL RESULTS 26

A. TEST PROCEDURE. 26

B. DATA RECORDING. 26

C. RESULTS 27

VII. CONCLUSIONS AND RECOMMENDATIONS 33

A. CONCLUSIONS 33

B. RECOMMENDATIONS 33

FIGURES 34

TABLES. 52

APPENDIX A: CALCULATION OF VELOCITIES. 54

APPENDIX B: EVALUATION OF THE PRESSURE COEFFICIENT. 55

APPENDIX C: TEST PROCEDURES SEQUENCE 56

APPENDIX D: SELECTED TEST DATA 58

LIST OF REFERENCES. 61

INITIAL DISTRIBUTION LIST 63

LIST OF FIGURES

II-1 Coordinate Conventions Used 34

II-2 Theoretical Pressure Distribution about a Cylinder and a Sphere 35

II-3 Pressure Distribution about a Cylinder in Subcritical and Supercritical Range of Reynolds Number. 36

II-4 Pressure Distribution about a Sphere in Subcritical and Supercritical Range of Reynolds Number. 36

II-5 Boundary Layer Separation and Vortex Formation on a Circular Cylinder (Diagrammatic). 37

III-1 Off-Turret Control 38

III-2 Slot Blowing Control 39

III-3 Base Suction with Trapped Vortices 40

III-4 Base Suction 41

III-5 Turret, Fairing, and Fuselage Boundary-Layer Suction. 42

IV-1 Aerovent Blower and Sheet Metal Mating Ducting 43

IV-2 Inlet Control Damper Assembly 43

IV-3 Fairing Duct Assembly and Plenum. 44

IV-4 Fairing Duct Assembly and Plenum (Installed) 45

IV-5 Fairing Nose Piece. 45

IV-6 Under-Tunnel Assembly (Right Side). 46

IV-7 Under-Tunnel Assembly (Left Side) 46

IV-8 Complete Model Assembly in Wind Tunnel (Side View) 47

IV-9 Complete Model Assembly in Wind Tunnel (Rear View) 47

V-1 Turret Pressure Tap Locations. 48

V-2 Wind Tunnel Data Acquisition System. 49

V-3 Scanning Valve 49

VI-1 Turret without Flow Control Suction 50

VI-2 Turret with Flow Control Suction. 50

VI-3 Turret Pressure Distribution with and without Flow Control Suction. 51

LIST OF TABLES

V-1 Instrumentation Pressure Tap Location List 52

VI-1 Estimated Q_r and ΔP_r for Full-Scale Applications at Various Altitudes 53

D-1 Test Data with Flow Control Off (Turbulent Flow) 59

D-2 Test Data with Flow Control On (Steady Flow) 60

ACKNOWLEDGEMENTS

I would like to acknowledge the assistance and support of Captain Richard deJonckheere, USAF, and the Air Force Weapons Laboratory for providing the funding necessary to conduct this research project. I would also like to thank my thesis partner, Lieutenant Alan Mandigo, for his assistance.

Most of all, I would like to express my sincere appreciation to Dr. Allen E. Fuhs, Distinguished Professor of Aeronautics and Physics and Chemistry. Dr. Fuhs' technical guidance, and his efforts as my Thesis Advisor, were crucial factors in the successful completion of this project. Also, I am grateful to have had the professional expertise of Professor T. H. Gawain as a second reader.

I would like to thank Supervisory Aerospace Engineering Technicians Robert Besel and Ted Dunton for their technical support in the use of the wind tunnel and its instrumentation. Additionally, I would like to express my appreciation for the work done by Model Shop Technician Ronald Ramaker. Without his expert precision-building of the turret and fairing models, this project could not have been completed. I would like to thank Lieutenant Commander Kenneth Tillotson, Lieutenant Commander Martin Mellor, and my wife, Lieutenant Rose Schonberger, for the time they donated in the preparation of the wind tunnel and model.

I. INTRODUCTION

A. BACKGROUND

A high-energy laser weapon system inflicts damage on a target by radiating large amounts of thermal energy onto a small area. The main components of the system are the laser, which generates high-power radiation, and the beam-control subsystem, which aims the laser beam at the target. The airborne portion of the Department of Defense (DoD) High Energy Laser (HEL) Program is being developed at the Air Force Weapons Laboratory, Kirtland Air Force Base, New Mexico. The test bed for the program is the Airborne Laser Laboratory (ALL), which consists of two highly-instrumented NKC-135 aircraft.

The laser beam is aimed at the target by the pointer tracker, which is part of the beam-control subsystem. The pointer tracker is housed on top of the aircraft, inside a laser turret. In flight, the airflow around the turret causes problems in beam control. The beam-control problems are jitter and optical path distortions (OPD). Jitter is a vibration of the laser beam that smears the energy focused within a small spot into a larger spot. The time required to damage the target is increased. Jitter is caused, in part, by unsteady pressure loads on the turret and optical components. Optical path distortions, steady and unsteady, are due to shear layers, boundary layers, flow separation, and vortex shedding in the rear of the turret. The flow around the turret also causes increased pressure loading in the separated-flow region behind the turret. This increased unsteady pressure is caused by turbulence within the recirculation region. The aiming of a laser through turbulence is a major problem.

Research and experimentation have demonstrated that optical distortion caused by unsteady flow cannot be corrected by adaptive optical systems. Bandwidth requirements exceed current technology.

B. THESIS OBJECTIVE

The primary objective of this thesis is to develop a quiescent airflow around the turret so that jitter and optical path distortions will be minimized. Control of flow separation will insure that flow will be quiescent well past the current 120-degree point, in order that a greater rearward angle can be achieved by the pointer tracker.

II. THEORETICAL FLOW OF INVISCID FLUIDS AND VISCOUS EFFECTS

A. POTENTIAL FLOW ABOUT A CYLINDER

The potential function, Φ, for uniform flow about a cylinder is given by:

$$\Phi = Ux + \frac{Ua^2x}{x^2 + y^2} \quad , \tag{2-1}$$

where U is the free-stream flow velocity and a is the radius of the cylinder. Figure II-1 illustrates the coordinate conventions used. Differentiating the potential function with respect to x and y yields the x and y components of velocity in the potential field:

$$u = \frac{\delta\Phi}{\delta x} = U + Ua^2\left\{\frac{y^2 - x^2}{(x^2 + y^2)^2}\right\}$$

$$v = \frac{\delta\Phi}{\delta y} = \frac{-Ua^2 2xy}{(x^2 + y^2)} \tag{2-2}$$

A change to plane cylindrical coordinates is helpful where $x = r\cos\theta$ and $y = r\sin\theta$. At the surface of the cylinder, $r = a$, and the surface velocity components, u and v, become:

$$u = 2U\sin^2\theta$$

$$v = -2U\sin\theta\cos\theta$$

Thus, the total surface velocity, V_s, is:

$$V_s = (u^2 + v^2)^{\frac{1}{2}} = 2U\sin\theta \quad . \tag{2-3}$$

Utilizing the surface velocity relation, the surface pressure distribution can be calculated. For an incompressible fluid, total pressure, P_0, is:

$$P_0 = P + \tfrac{1}{2}\rho V^2 \quad . \tag{2-4}$$

At infinity, $V = U$; and, at the surface, $V = V_s$. Therefore:

$$P_0 = P_\infty + \tfrac{1}{2}\rho U^2 = P_s + \tfrac{1}{2}\rho V_s^2$$

$$P_s - P_\infty = \tfrac{1}{2}\rho (U^2 - V_s^2) \tag{2-5}$$

The free-stream dynamic pressure, q, is defined as:

$$q = \tfrac{1}{2}\rho U^2 \quad . \tag{2-6}$$

Substituting Eq. 2-3 and Eq. 2-6 into Eq. 2-5 yields the surface pressure distribution for a cylinder:

$$\frac{P_s - P_\infty}{q} = \frac{\Delta P}{q} = 1 - 4\sin^2\theta \quad . \tag{2-7}$$

The ratio in Eq. 2-7 is the pressure coefficient.

Figure II-2 is a plot of the pressure distribution expressed in Eq. 2-7, as well as a plot of the pressure distribution about a sphere, as developed below.

B. POTENTIAL FLOW ABOUT A SPHERE

The potential function for uniform flow in spherical coordinates about a meridian section of a sphere of radius a is:

$$\Phi = U(r\cos\theta + \frac{a^3\cos\theta}{2r^2}) \quad . \tag{2-8}$$

As before, at the surface, $r = a$, and the surface velocity components, u and v, become:

$$u = \frac{\delta\Phi}{\delta r} = U(\cos\theta - \frac{a^3\cos\theta}{a^3})$$

$$v = \frac{1}{r}\cdot\frac{\delta\Phi}{\delta\theta} = -\frac{3}{2}U\sin\theta$$

Total surface velocity, V_s, is therefore:

$$V_s = \frac{3}{2}\cdot U\sin\theta \quad . \tag{2-9}$$

Substituting Eq. 2-9 and Eq. 2-6 into Eq. 2-5 yields the surface pressure distribution for a sphere:

$$\frac{P_s - P_\infty}{q} = \frac{\Delta P}{q} = 1 - \frac{9}{4}\sin^2\theta \quad . \tag{2-10}$$

Equation 2-10 is plotted in Figure II-2.

C. VISCOUS EFFECTS AND FLOW SEPARATION

The preceding potential flow theory dealt with the flow of a perfect (inviscid) fluid. An inviscid fluid is satisfactory from a mathematical

standpoint in that the equations, which offer some insight into the flow pattern, can be solved readily. However, real effects, such as drag and turbulence, are not predicted by this theory. Experimental measurements indicate significant variance from theory, and the degree of variance is strongly dependent upon the Reynolds number, Re. The Reynolds number is defined as VD/ν, where V is velocity, D is diameter, and ν is kinematic viscosity, all quantities being measured in consistent units. Only in the limiting case, as $Re \to \infty$ (i.e., $\nu \to 0$), does theory agree with experiment, since $\nu = 0$ implies inviscid flow. Figures II-3 and II-4 depict theoretical static pressure distribution, along with actual experimental data for a cylinder and a sphere, respectively.

Since all real fluids are viscous, the fluid adheres to a wall (or boundary) in the flow, and frictional forces retard the motion of the fluid in a thin layer along the wall. In this thin layer, the velocity of the fluid increases from zero at the wall to the full free-stream velocity in a short distance. The boundary layer was first described by L. Prandtl, and accounts for the phenomena of skin friction drag and boundary layer turbulence. [2]

The boundary layer separation at high Reynolds numbers, which may result in turbulence, can be explained by considering the flow about a blunt object, e.g., a circular cylinder (or laser turret). Figure II-5 shows a stylized flow pattern about a cylinder and the corresponding pressure distribution of potential flow. Outside the boundary layer, the flow accelerates from A to B, and the static pressure decreases. Likewise, the flow decelerates from B to C, and the static pressure increases. The decrease in static pressure from A to B is converted into dynamic pressure,

which is then converted back into static pressure from B to C, such that the velocities and total pressures at A and C are equal. However, within the boundary layer, considerable friction exists. Furthermore, the external pressure is impressed upon the boundary layer. Because of the frictional forces in the boundary layer, the boundary layer fluid consumes some of the kinetic energy (dynamic pressure) from A to B. As a consequence, not enough energy remains to overcome the impressed static pressure gradient from B to C. Eventually, motion of the boundary layer fluid is arrested, and the external static pressure causes the boundary layer fluid to move in the opposite direction. Thus the flow separates, and, in a separated flow region at high Reynolds number, the flow becomes turbulent. The separation point, S, is not a fixed point, but is dependent upon the Reynolds number and the shape of the body. By reducing or eliminating the pressure gradient from B to C, the separation point could be moved (in theory) to the vicinity of point C, and the flow external to the boundary layer would remain steady. The concept of flow control using a favorable pressure gradient is the essence of the research presented in this thesis.

III. FLOW CONTROL

A. SURVEY OF VARIOUS PROPOSED METHODS

The following proposed methods were presented at a workshop entitled "Control of Turbulent, Separated Airflow about Aircraft Turrets," sponsored by Captain Richard deJonckheere at the Air Force Weapons Laboratory, Kirtland Air Force Base, Albuquerque, New Mexico, on 10 and 11 March 1980.

1. Off-Turret Control

The method of off-turret control uses suction through a porous standpipe at the rear of the turret. The suction is used to achieve quiescent airflow around the turret. Figure III-1 is a side view of the off-turret control method. The forward fairing, if installed, would be used to eliminate vorticity at the turret-fuselage junction.

2. Slot Blowing

The slot blowing method attempts to keep the airflow attached to the turret by the use of jets of air. The jets are located at various points on the turret. Figure III-2 is a top view of the geometry for the slot blowing method; the figure also shows the difference between flow with blowing and flow without blowing. The ducting required for the airjets, of course, complicates turret design.

3. Base Suction with Trapped Vortices

This method uses suction through ports on both sides of a fairing located very close to the turret. The suction is used to create, stabilize, and remove vorticity shed into the wake. Figure III-3 is a top and side view of the apparatus used in this method. Note the design of the fairing.

4. Base Suction

The base suction method uses suction through an array of small holes at the rear of the turret. The suction removes the boundary layer formed on the turret. Figure III-4 is a top view of the base suction method. This is an efficient method, but it complicates turret design. The complications arise from the fact that the turret turns, but the suction holes must remain downstream in order to establish and preserve a steady flow.

B. TEST METHOD

The fairing and base-suction apparatus used were designed specifically for this research project. The hardware consists of the turret, fuselage boundary layer bleed, hollow fairing, fairing nose piece, and a blower. The specifications and designs are covered in Chapter IV.

The fairing and base suction apparatus employ suction through a hollow fairing and fairing nose piece behind the turret. Quiescent airflow around the turret is achieved due to the suction. Figure III-5 is a top and side view of the turret, fairing, and fuselage boundary layer bleed.

IV. EXPERIMENTAL APPARATUS

A. WIND TUNNEL

Wind tunnel tests were conducted in the Naval Postgraduate School's five-foot by five-foot low-speed tunnel at a maximum velocity of 33 feet per second, allowing a Reynolds number per foot of 2.06×10^5. The five-foot by five-foot tunnel was chosen due to availability and physical size. With the one-third scale turret model (D = 16.8 inches) a Reynolds number of about 3×10^5 was achieved. According to Schlichting [2], the value of the Reynolds number for the tests was in the critical range, and turbulent flow was predicted.

B. BLOWER SPECIFICATIONS

The blower which provides the fairing suction was selected based on flow rate, measured in cubic feet per minute (ft^3/min), and on pressure differential, measured in inches of water (in. H_2O). Initial calculations, utilizing the proposed fairing inlet area and a velocity equal to twice free-stream velocity, yielded a flow rate of 7,200 ft^3/min. Twice the free-stream velocity was chosen based on potential flow theory for flow about a cylinder. Potential flow theory also provided the required pressure differential. In order to eliminate the adverse pressure gradient behind the turret model, a minimum pressure differential of three times the free-stream dynamic pressure was desired. Using a free-stream velocity of 40 feet per second, free-stream dynamic pressure is approximately 0.36 in. H_2O. To allow for losses within the ducting, and to provide flexibility

in possible follow-on experiments with higher velocities and pressure differentials, blower specifications were increased. The final specifications submitted to manufacturers for bids were for a flow rate of not less than 7,500 ft^3/min and a pressure differential of not less than 14 in. H_2O. Additional specifications included size restrictions and inlet flow control dampers.

The Aerovent Company, Inc., of Piqua, Ohio, was selected as the blower manufacturer, as their Backward Inclined Airfoil, Model 500, Single-Width Single-Inlet (B.I.A.-500, SWSI) centrifugal blower met or exceeded all specifications. The Aerovent blower has a capacity of 7,700 ft^3/min with a static pressure differential of 14 in. H_2O. Figure IV-1 is a photograph of the Aerovent blower and the sheet metal which mates the blower to the ducting. The inlet control damper assembly is shown in Figure IV-2, which is a view looking into the mating duct.

C. FAIRING DESIGN

A hollow fairing with four internal ducts was constructed; each duct contained a butterfly valve to throttle the flow. The fairing dimensions were such that a maximum turret look-back angle of 150 degrees could be obtained. Pitot-static tubes were installed in each duct for measurement of flow velocities. Provisions were made for a detachable fairing nose piece to allow variation of the turret/fairing geometry. Additionally, a plenum allowing for fuselage boundary layer suction at the base of the turret was incorporated into the fairing assembly. Figure IV-3 shows the fairing duct assembly and plenum. Figure IV-4 shows the fairing duct assembly and under turret plenum after installation in the wind tunnel and

without the nose piece attached or the turret installed. Note the plenum for fuselage boundary layer suction.

D. FAIRING NOSE PIECE DESIGN

A tapered, symmetric nose piece was constructed with variable-area inlets on each side. A splitter plate, which isolates the flow around each side of the turret, was an integral part of the design. Figure IV-5 shows the nose piece ready for installation. Note the variable-area side inlets and the splitter plate.

E. TURRET DESIGN

A stylized, one-third scale model of the existing airborne laser turret was constructed, based on drawings provided by Captain deJonckheere of the Air Force Weapons Laboratory (AFWL). The model consists of a hollow, 16.8 inch diameter right circular cylinder, 9.6 inches in height, topped by a 16.8 inch diameter hemisphere. The turret is mounted on 0.375 inch aluminum plate, with a slot for fuselage boundary layer suction.

F. MODEL INSTALLATION

The blower, with the sheet metal which mates the blower to the ducting, was mounted beneath the wind tunnel test section. The test section floor was removed, and the fairing assembly was installed in the test section and mated to the blower assembly. Figures IV-6 and IV-7 are two views of the under-tunnel assembly. Note the flow control damper handles in the duct assembly in Figure IV-7. Figures IV-8 and IV-9 are photographs of the complete model assembly in the tunnel test section.

V. INSTRUMENTATION

A. PRESSURE TAPS

Pressure taps were installed on the turret, in the wind tunnel, and in the duct assembly. As a result of the extensive array of pressure taps, the pressure distribution on the turret surface could be plotted. Knowledge of static pressure permits calculation of local velocity. Table V-1 is a list of the locations of the pressure taps. Figure V-1 is a top- and side-view drawing of the turret, giving exact pressure tap locations. The locations of the pressure lines attached to the five pitot-static tubes of the under-tunnel duct assembly can be seen in Figure IV-6. These lines are for static and dynamic pressure.

B. WIND TUNNEL DATA ACQUISITION SYSTEM

The wind tunnel data acquisition system used in this research project consisted of an INTEL 80/10 computer system, an AN/UGC-59A teletypewriter set, a 48-port Scanivalve, and a digital display unit for the Scanivalve. Figure V-2 is a photograph of the computer system, teletypewriter, and digital display unit. Figure V-3 is a photograph of the Scanivalve.

A control program for the Scanivalve was developed so that the pressure at each of the 48 ports could be measured. Each port of the Scanivalve was attached to its corresponding pressure tap via Tygon plastic tubing.

The measured quantity for each pressure tap is a dimensionless number; in the experiments, it was proportional to the voltage across a capacitor

pressure transducer located in the bottom of the Scanivalve. To convert the Scanivalve output values to a more useful form, the following calibration procedure was used: With a U-tube water manometer, readings were taken and plotted for each centimeter of water pressure from zero to ten. The plot determined that the Scanivalve output was linear with pressure, and a least-squares plot of best fit was calculated, such that

$$y = mx + b \quad , \tag{5-1}$$

where y is pressure, in centimeters of water, and x is the dimensionless measured value. From the calibration procedure, numerical values for m and b were obtained. The results were $m = 9.2608$ and $b = 0.0269$. The pressure readings were used to calculate the pressure coefficients and the velocities in the wind tunnel and ducting. Appendix A is an outline of the procedure used to calculate velocities, and Appendix B is an outline of the procedure used to find the pressure coefficients.

C. TUFTS

In order to evaluate qualitatively the steadiness of the airflow, horizontal rows of tufts were taped to the turret. These tufts were made of a light yarn so that small airflow velocities caused displacement of the tufts. If the flow around the turret was turbulent, the tufts would be unsteady and in a state of disarray. When the flow was quiescent, the tufts would lie flat in the direction of the flow.

VI. EXPERIMENTS AND EXPERIMENTAL RESULTS

A. TEST PROCEDURE

A test sequence was developed based on the requirement to investigate the following parameters: (1) turret position relative to the fairing; (2) fuselage boundary layer suction; (3) fairing inlet area; (4) total blower suction; and (5) control of fairing suction through the individual ducts. The test sequence included a step-by-step procedure to determine the combination of test variables which provide optimum flow stability. Optimum conditions were steady flow with the minimum amount of suction. These conditions were determined by tuft steadiness and turret pressure gradient measurements. Appendix C gives the test sequence used.

B. DATA RECORDING

When the desired wind tunnel conditions were attained, the data acquisition system was triggered manually. The data acquisition system was described in detail in the preceding chapter. The pressure ratio, $\Delta P/q$, was calculated for each turret pressure tap and plotted against port position. Reference static pressure, P_∞, was measured at the wind tunnel wall, near the turret position (port number 38). Reference dynamic pressure, q, was measured with an impact probe (port number 43) adjacent to the tunnel wall pressure port. Observations of tuft steadiness were recorded as well, and a color sixteen-millimeter movie of a test run, with and without flow control employed, was made.

C. RESULTS

The turret pressure distribution with no flow control was measured as a baseline for comparison before the test sequence was started. (Test data are included in Table D-1.)

The IA test series indicated that total blower suction of not less than 50% capacity (approximately 4,000 ft^3/min) is required for steady flow. See Appendix C for identification of tests. The maximum fairing inlet area available is 1.0 ft^2 with the adjustable cover plates in the open position. The tests, in this sequence, show that a fairing inlet area of greater than 0.5 ft^2 is required. The best flow in this series resulted when total blower suction of 50% and a fairing inlet area of 0.75 ft^2 were employed.

The IB series of tests indicated no improvement in flow conditions when individual duct suction rates were varied. The optimum setting of the duct butterfly valves was therefore determined to be the fully-open position.

The IIA series of tests resulted in a clear improvement in flow when fuselage boundary layer suction was employed. Fuselage suction inlet area was varied in series IIB. Optimum flow resulted with a fuselage suction inlet area of 0.12 ft^2, a fairing inlet area of 0.75 ft^2, total blower suction at 4,000 ft^3/min, and all butterfly valves fully open. (Data from Test #1 of the IIB series are included in Table D-2.)

Test series IIIA and IIIB, with the rear of the turret located 4 inches forward of the fairing, indicated less stable flow. Therefore, Test #1 of the IIB series was selected as the overall optimum flow condition. Figure VI-1 is a photograph of the turret with the wind tunnel on

but without flow control suction; note the disarray of the tufts. Contrast this with Figure VI-2, which is a photograph of the turret with both the wind tunnel and the flow control activated; note the steadiness of the tufts with flow control employed.

The turret pressure distribution from Test #1 of the IIB series is plotted in Figure VI-3. Also plotted in Figure VI-3 is the pressure distribution without flow control (curve 1) and the pressure distribution from potential flow theory (curve 2). The distributions from Test #1 of the IIB series are those about the spherical portion (curve 3) and the cylindrical portion (curve 4) of the turret, while the other distributions are those about the cylindrical portion only. The cylindrical portion was used as a baseline for comparison, since the separated flow was most difficult to control in this region. Comparing the pressure distribution without flow control (curve 1) against Figure II-3, the distribution agrees well with historical experiment.

In Figure VI-3, the adverse (increasing) pressure gradient from the 90° point to the 180° point can be seen (curve 1). However, with the flow control suction employed (curves 3 and 4), a favorable gradient exists at least to the 135° point. The dotted line from the 135° point to the 180° point (curve 4) is an attempt to extrapolate the pressure gradient between 135° and 180°. Without pressure taps in this region, the exact gradient is not known. However, based on tuft observations, the flow appears to remain steady to at least the 150° point, which implies that the favorable pressure gradient may extend beyond the 135° point.

The accuracy of pitot-static measurements of velocities within the duct system during testing was questionable. A high degree of variance

in velocity was noted between the tests using the pitot-static measurements. Therefore, an alternate method of estimating the inlet velocities was used. This method is based on mass flow rate (Q), area ratios, and velocity ratios, as follows:

$$Q = V_b A_b = V_1 A_1 + V_2 A_2 + V_3 A_3 + V_4 A_4 + V_5 A_5 \tag{6-1}$$

The subscripts refer to the numbers assigned to the various suction ducts, while b refers to the blower inlet. Subscripts 1 through 4 refer to the fairing ducts from top to bottom, while subscript 5 refers to the fuselage boundary-layer duct. Rearranging Eq. 6-1 yields:

$$\frac{V_1 A_1}{V_b A_b} + \frac{V_2 A_2}{V_b A_b} + \frac{V_3 A_3}{V_b A_b} + \frac{V_4 A_4}{V_b A_b} + \frac{V_5 A_5}{V_b A_b} = 1 \quad .$$

The pressure relation, $P_0 - P_i = \frac{1}{2}\rho V_i^2$, is solved for V_i. Also, P_0, which is equal to $P + q$, is a constant.

The velocity ratio, V_i/V_j, is formed, which yields:

$$\frac{V_i}{V_j} = \left[\frac{1 + (P - P_i)/q}{1 + (P - P_j)/q}\right]^{\frac{1}{2}} = \left[\frac{1 - \Delta P_i/q}{1 - \Delta P_j/q}\right]^{\frac{1}{2}} \quad . \tag{6-2}$$

Solving Eq. 6-1 for V_1/V_b results in an expression of velocity ratios which can be calculated from Eq. 6-2 and the known area ratios:

$$\frac{V_1}{V_b} = \left[\frac{A_1}{A_b} + \frac{V_2 A_2}{V_1 A_b} + \frac{V_3 A_3}{V_1 A_b} + \frac{V_4 A_4}{V_1 A_b} + \frac{V_5 A_5}{V_1 A_b}\right]^{-1} \quad . \tag{6-3}$$

The pressure ratios, $\Delta P_i/q$, can be estimated using interpolated values for the midpoint of each inlet based on measured pressure ratios at the 180°

point on the turret. The estimated values for Test #1 of the IIB series were: $\Delta P_1/q = -2.15$, $\Delta P_2/q = -2.20$, $\Delta P_3/q = -2.10$, $\Delta P_4/q = -1.5$, and $\Delta P_5/q = -1.5$. These values of pressure ratios yield, from Eq. 6-2: $V_2/V_1 = 1.008$, $V_3/V_1 = 0.992$, $V_4/V_1 = 0.845$, and $V_5/V_1 = 0.845$.

Inlet areas were measured, and their ratios to the blower inlet area yielded: $A_1/A_b = 0.0455$, $A_2/A_b = 0.0530$, $A_3/A_b = 0.1364$, $A_4/A_b = 0.0265$, and $A_5/A_b = 0.0379$. Equation 6-3 was solved using the above data, which gave $V\ /V_b = 3.465$.

The blower inlet velocity, V_b, was estimated using data provided by the blower manufacturer for Q with the inlet damper set at 50% open, which yielded a Q of 4,000 ft^3/min (66.67 ft^3/sec).

$$V = \frac{Q\ (ft^3/sec)}{A_b} = \frac{66.67}{2.64} = 25.25\ ft/sec$$

Therefore, $V_1 = 87.5$ ft/sec, $V_2 = 88.2$ ft/sec, $V_3 = 86.8$ ft/sec, $V_4 = 73.9$ ft/sec, and $V_5 = 73.9$ ft/sec. These values of inlet velocity, when compared with the free-stream tunnel velocity of 32.7 ft/sec, indicate an inlet velocity range of 2.25 to 2.70 times that of the free-stream velocity.

The cross-sectional area of the upstream streamtube, A_∞, in the wind tunnel corresponding to Q was computed:

$$A_\infty = \frac{Q}{V_\infty} = \frac{66.67}{32.7} = 2.04\ ft^2$$

The value of A_∞ was compared with the presented area of the turret, A_t. The value of A_t for the model was 1.9 ft^2. The area factor, F, is defined as:

$$F = \frac{A_\infty}{A_t} = 1.07 \quad .$$

The area factor was used in scaling this test data to the actual aircraft configuration at a flight velocity, $M_\infty = 0.5$.

The required flow rate, Q_r, was determined for incompressible flow to be:

$$Q_r = Fa_\infty M_\infty A_t \text{ (60 sec/1 min) ft}^3\text{/min} \quad , \tag{6-4}$$

where A_t now represents the full-scale turret presented area. The value of A_t for the full-scale turret is 17.1 ft^2.

The required pressure differential, ΔP_r, for the aircraft suction device was estimated based on the turret pressure differential from the 135° point to ambient. An assumption of 70% pressure recovery in a fairing diffuser, π_r, was made, resulting in a pressure differential factor, n.

$$n = (1 - \pi_r) \cdot \left(\frac{\Delta P}{q}\right)_{135°} = (0.3) \cdot (4.7) = 1.41$$

$$\Delta P_r = nq = n \cdot \frac{\gamma}{2} \cdot P_\infty M_\infty^2 \tag{6-5}$$

The values of Q_r and ΔP_r for various altitudes were computed using Eq. 6-4 and Eq. 6-5, and are tabulated in Table VI-1. Pressure and sound velocity at altitude are from Ref. 4.

The tabulated results for Q_r were computed for incompressible flow. In order to estimate the minimum required fairing inlet suction area, A_g, and considering compressibility effects, choked flow was assumed at the inlet, i.e., $A_g = A^*$. Liepmann and Roshko [5] list the area ratio for

choked flow at $M = 0.5$ as $A^*/A_\infty = 0.7464$. With $A_\infty = 1.07 \cdot A_t = 18.3\ ft^2$, $A_g = 0.7464 \cdot A_t = 13.66\ ft^2$. However, the fairing inlet area of the test model, if scaled up to full size, would be $7.83\ ft^2$. The above computation indicates, therefore, that a larger fairing inlet area would be required for the actual aircraft configuration.

VII. CONCLUSIONS AND RECOMMENDATIONS

A. CONCLUSIONS

The concept of providing after-body suction as a means of flow control has proven effective, at critical Reynolds number, in incompressible flow. The application of after-body suction in transonic, compressible flow at super-critical Reynolds number has not yet been demonstrated, but with testing at transonic velocities, the concept could be proven or disproven. If proven, the requirements for flow control for the Airborne Laser could be met utilizing this concept. Other applications of after-body flow control, such as control about a Forward-Looking Infra-Red (FLIR) turret, may be realized as well.

B. RECOMMENDATIONS

Testing at transonic velocities will be required to demonstrate the feasibility of flow control by after-body suction in airborne systems. Other turret/fairing geometries should be tested to achieve a maximum beam look-back angle while minimizing suction requirements. Laser beam quality with flow control employed also should be examined.

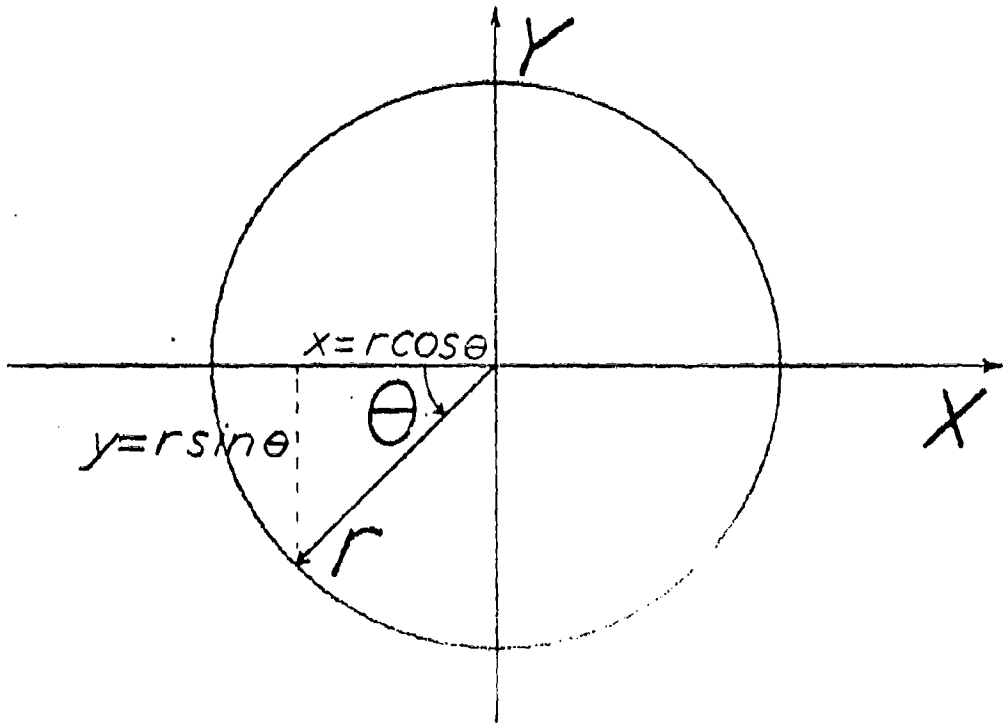

Figure II-1. Coordinate Conventions Used

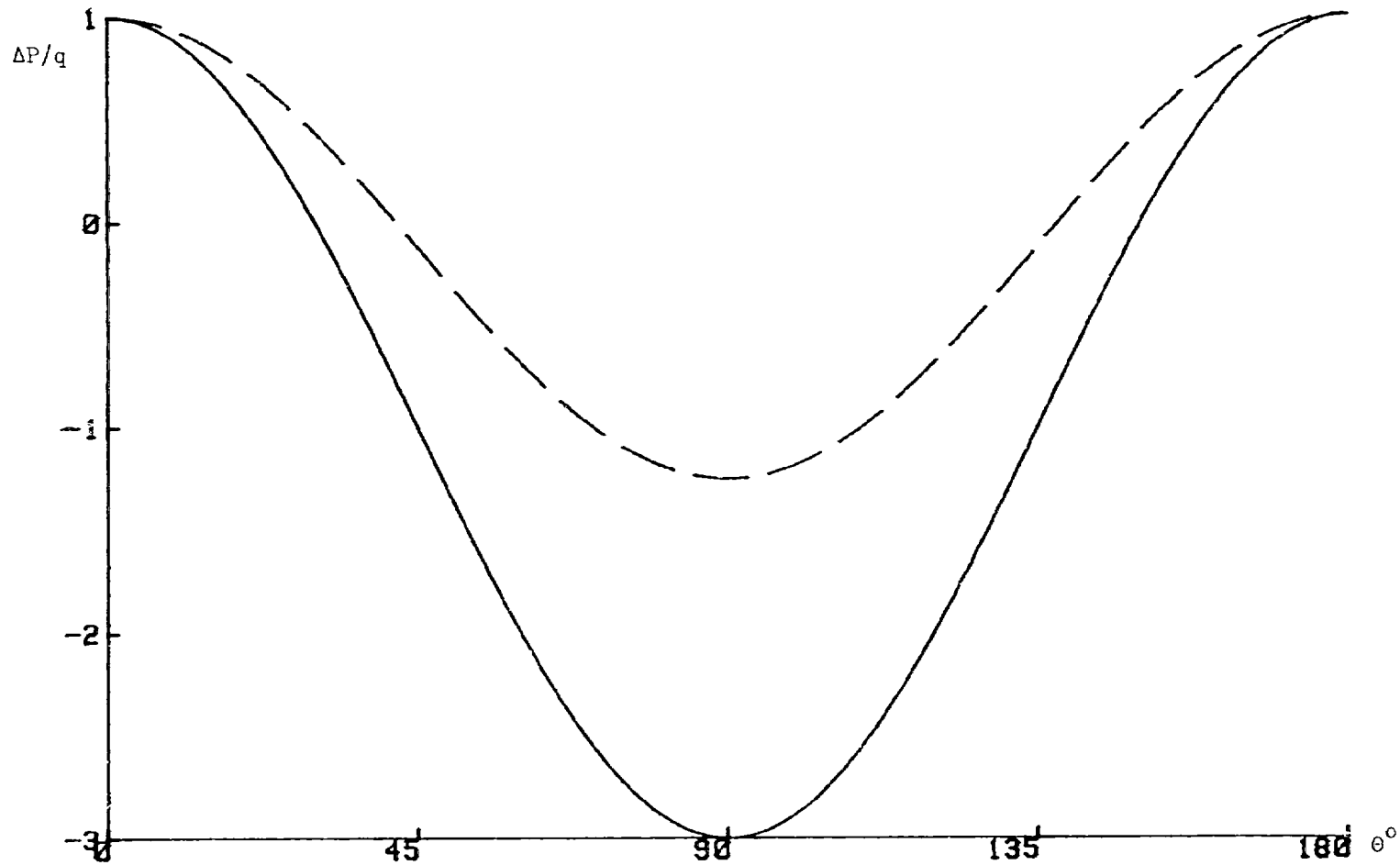

Figure II-2. Theoretical Pressure Distribution about a Cylinder (Solid) and a Sphere (Dashed)

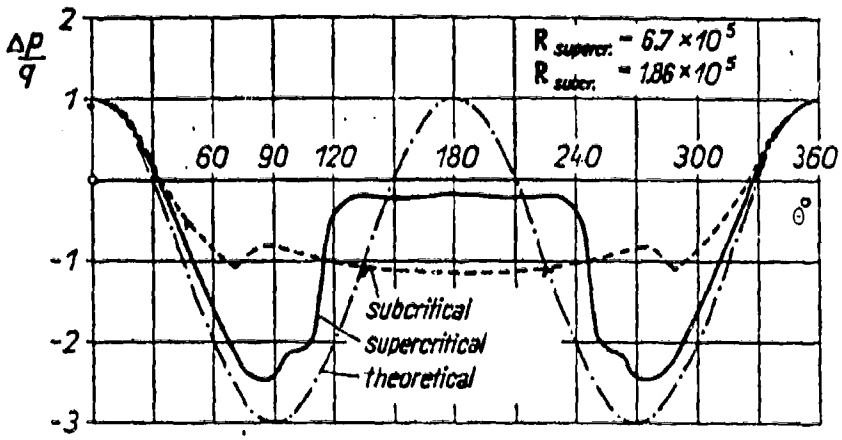

Figure II-3. Pressure Distribution about a Cylinder in Subcritical and Supercritical Range of Reynolds Number, from Schlichting [2] p. 21

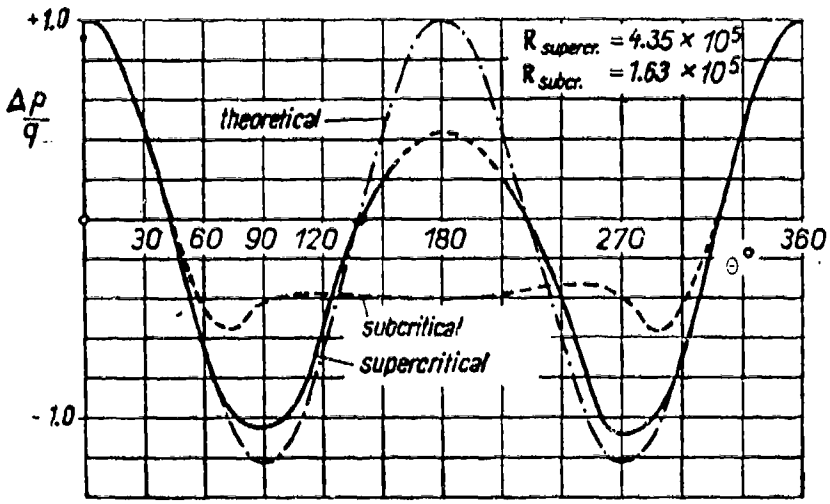

Figure II-4. Pressure Distribution about a Sphere in Subcritical and Supercritical Range of Reynolds Number, from Schlichting [2] p. 21

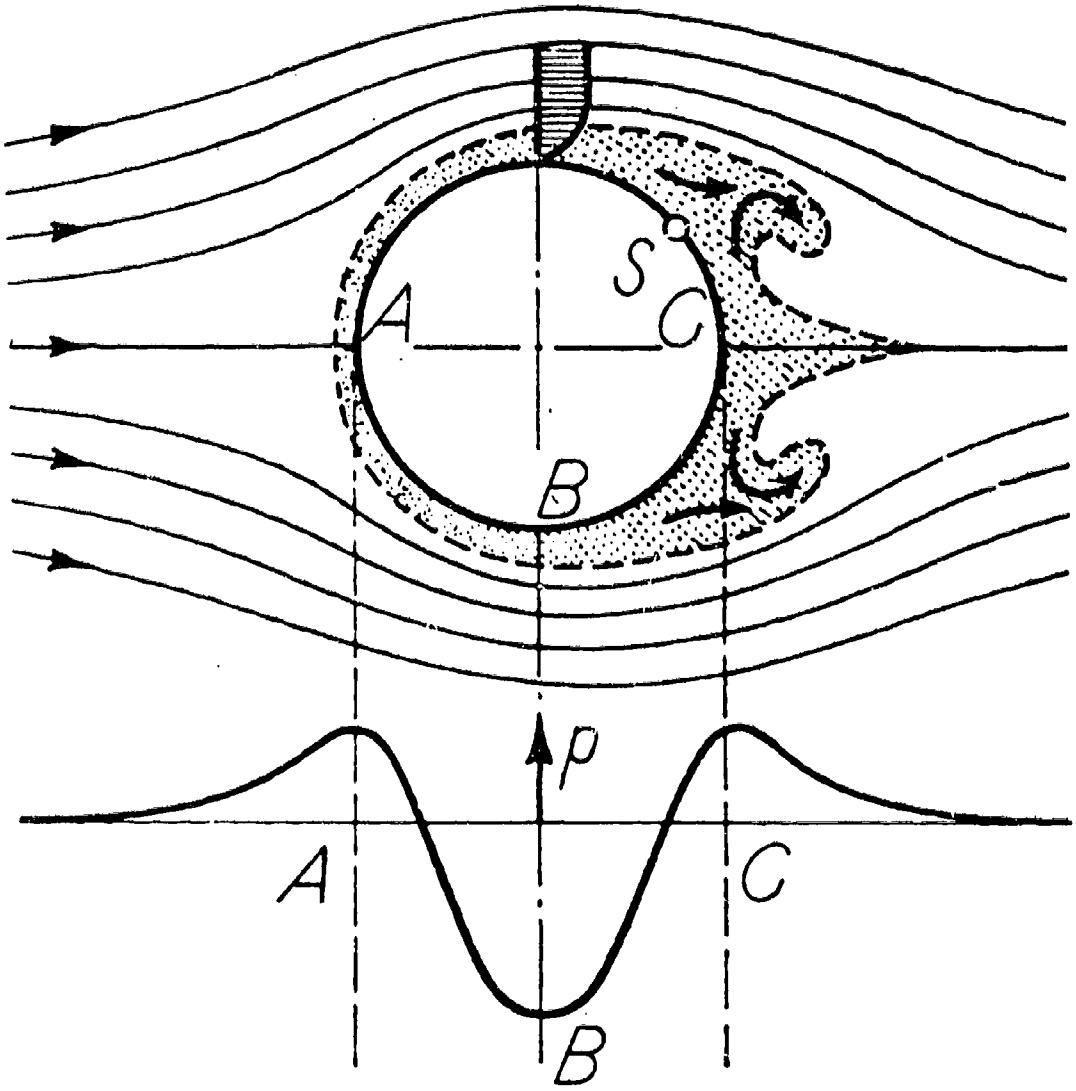

Figure II-5. Boundary Layer Separation and Vortex Formation on a Circular Cylinder (Diagrammatic), from Schlichting [2] p. 29

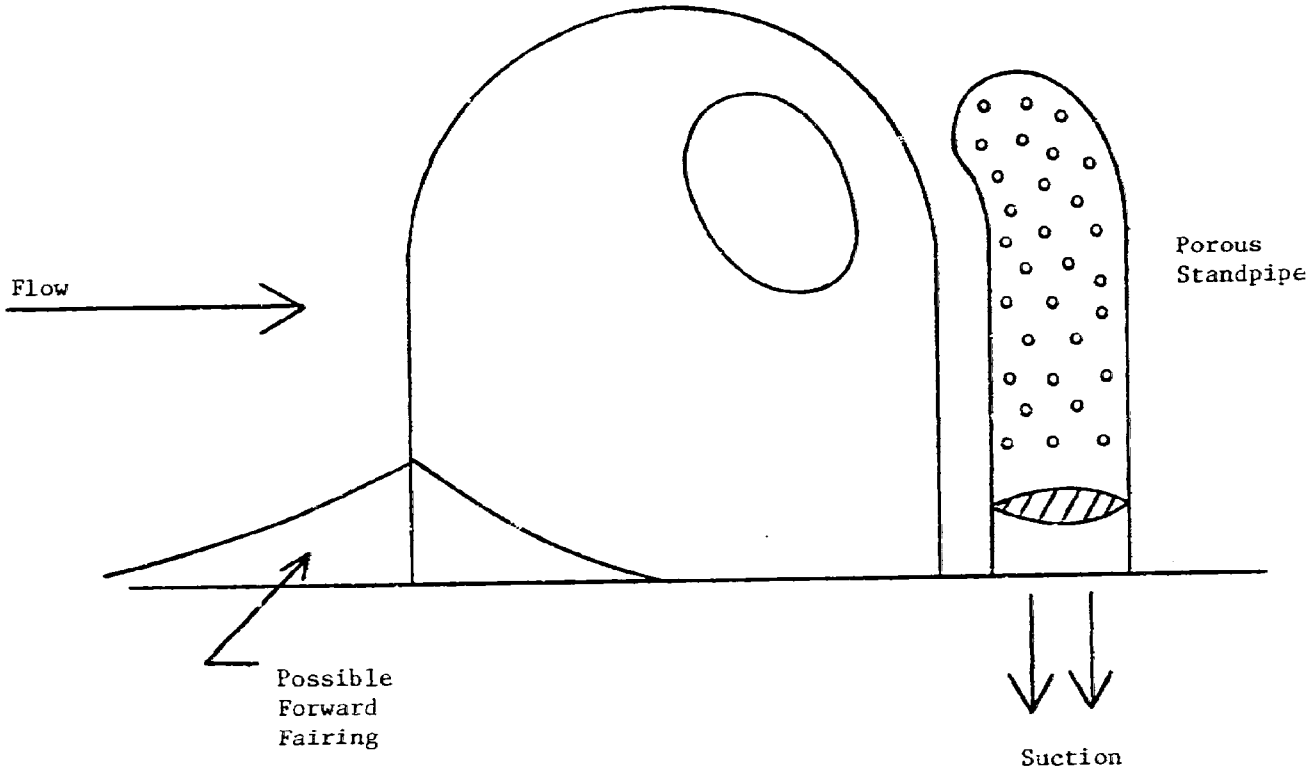

Figure III-1. Off-Turret Control
from deJonckheere [3]

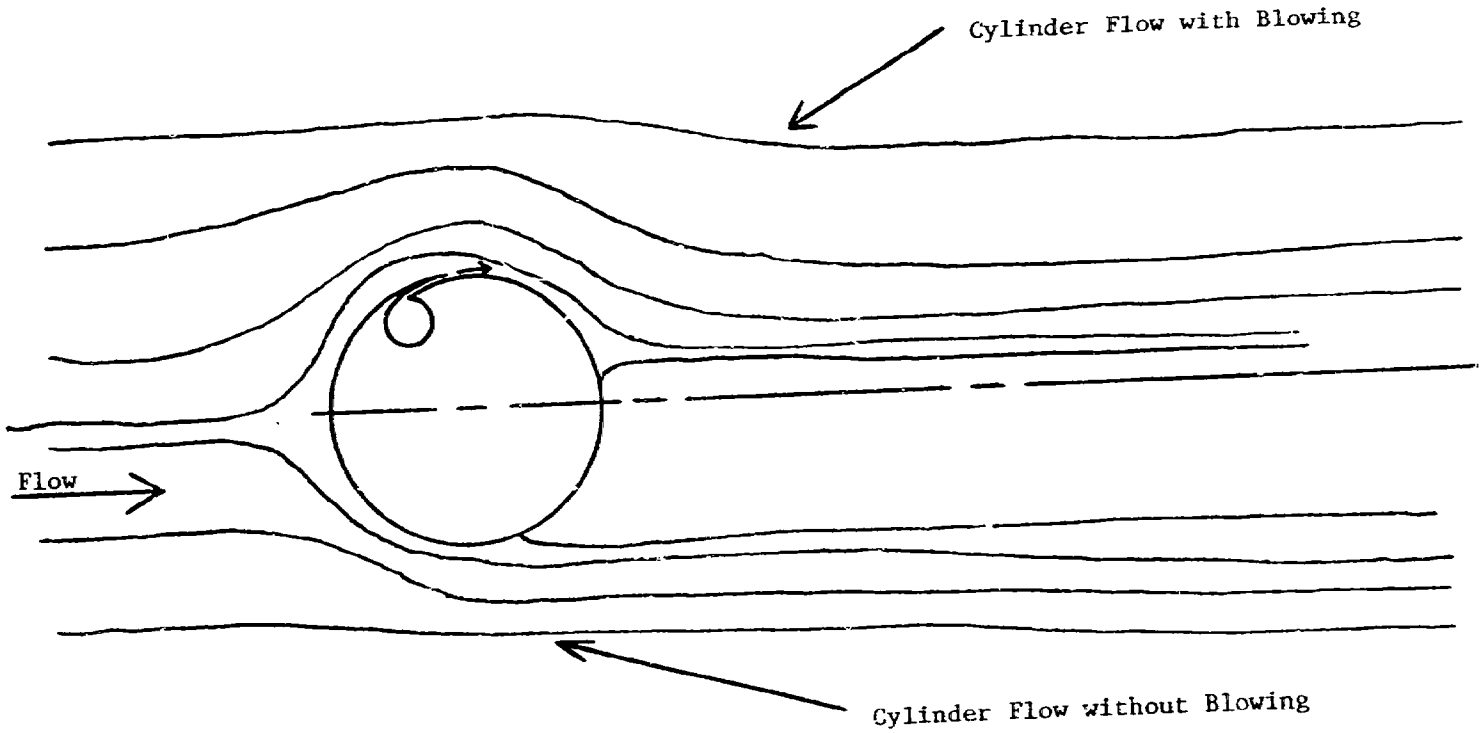

Figure III-2. Slot Blowing Control
from deJonckheere [3] , presented by
Spectron Development Laboratories Inc.

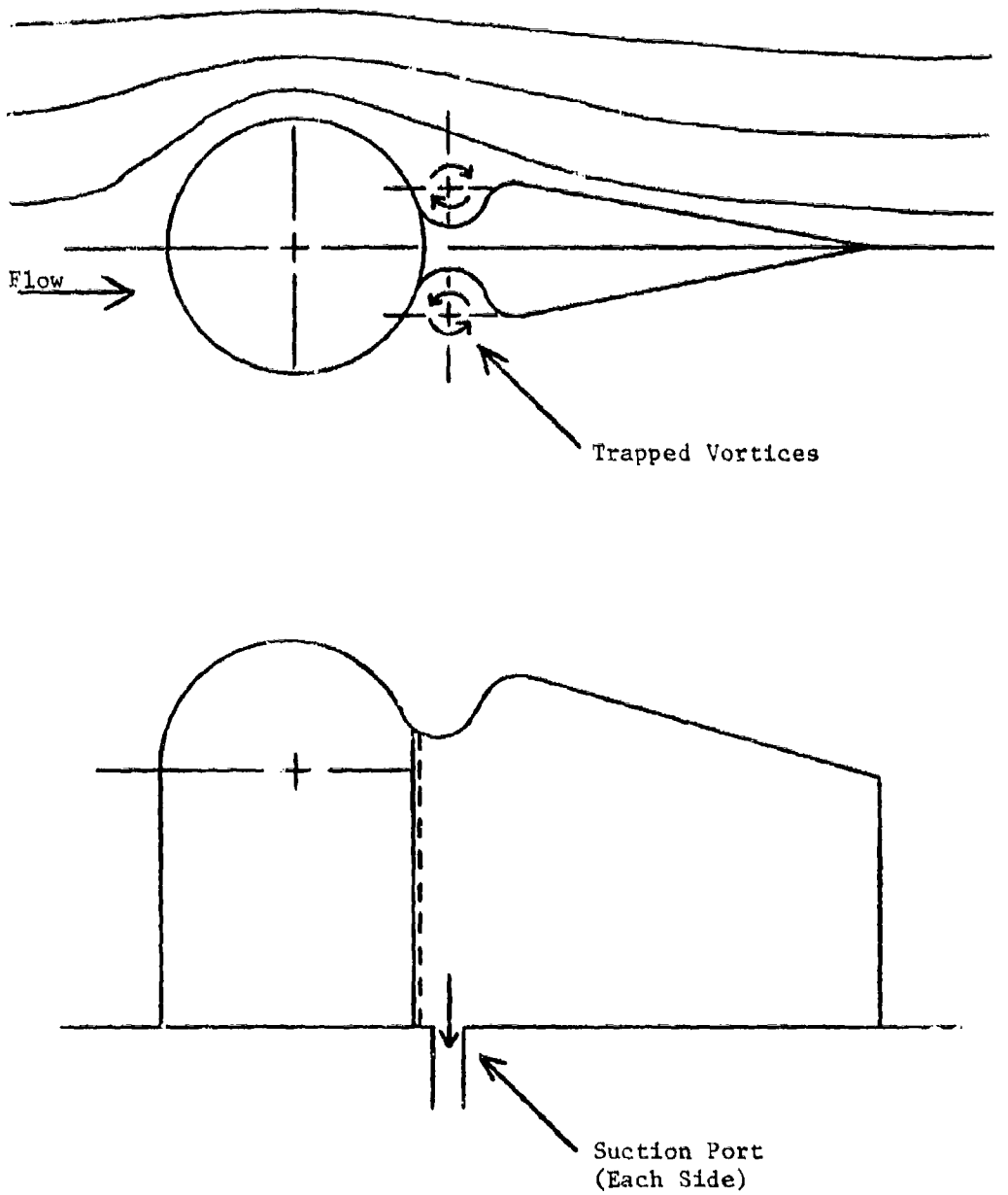

Figure III-3. Base Suction with Trapped Vortices from deJonckheere [3] , presented by Spectron Development Laboratories, Inc.

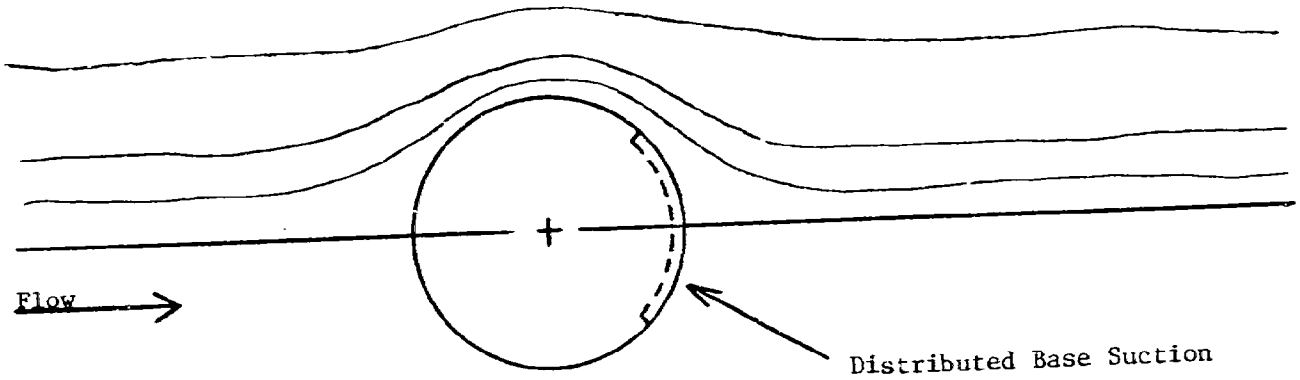

Figure III-4. Base Suction
from deJonckheere [3] , presented by
Spectron Development Laboratories, Inc.

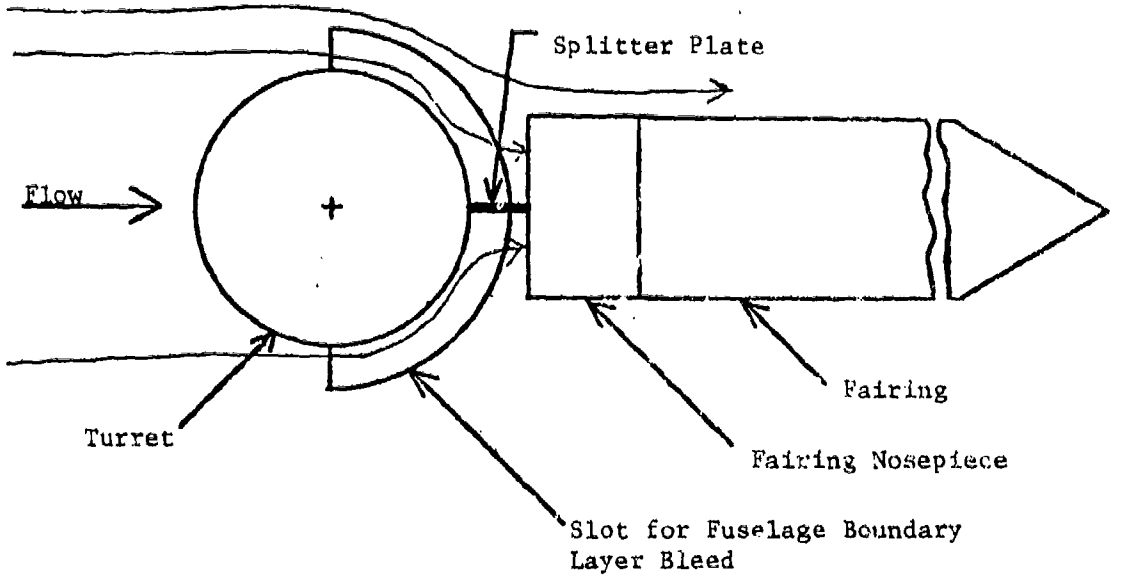

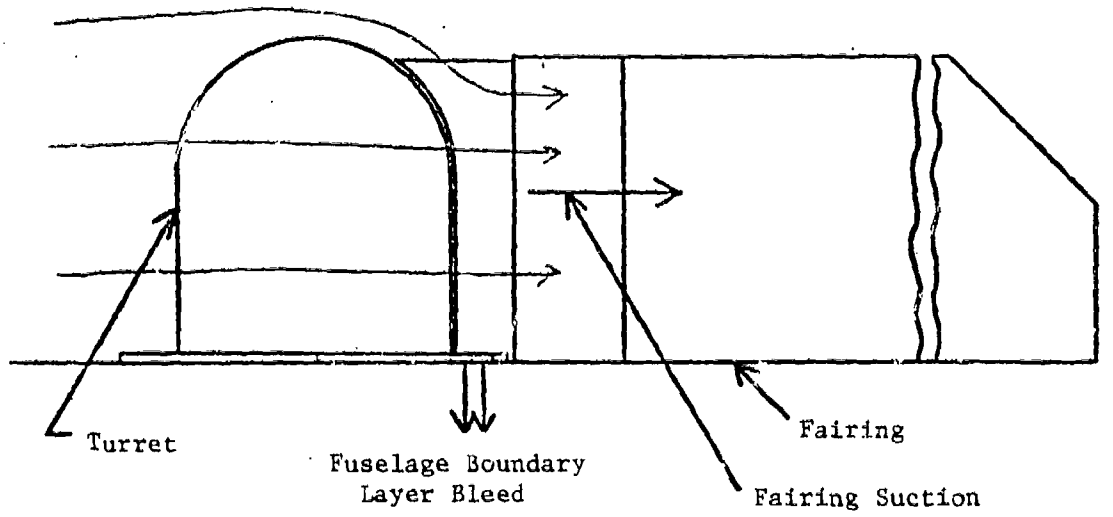

Base and Fairing Suction provided by blower mounted at the base of the fairing and connected via ducting.

Figure III-5. Turret, Fairing, and Fuselage Boundary Layer Suction

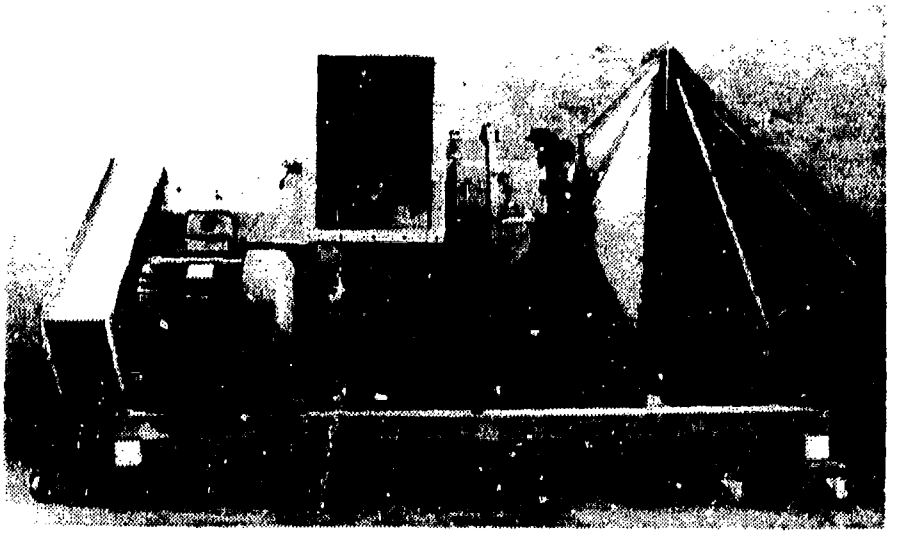

Figure IV-1. Aerovent Blower and Sheet Metal Mating Ducting

Figure IV-2. Inlet Control Damper Assembly

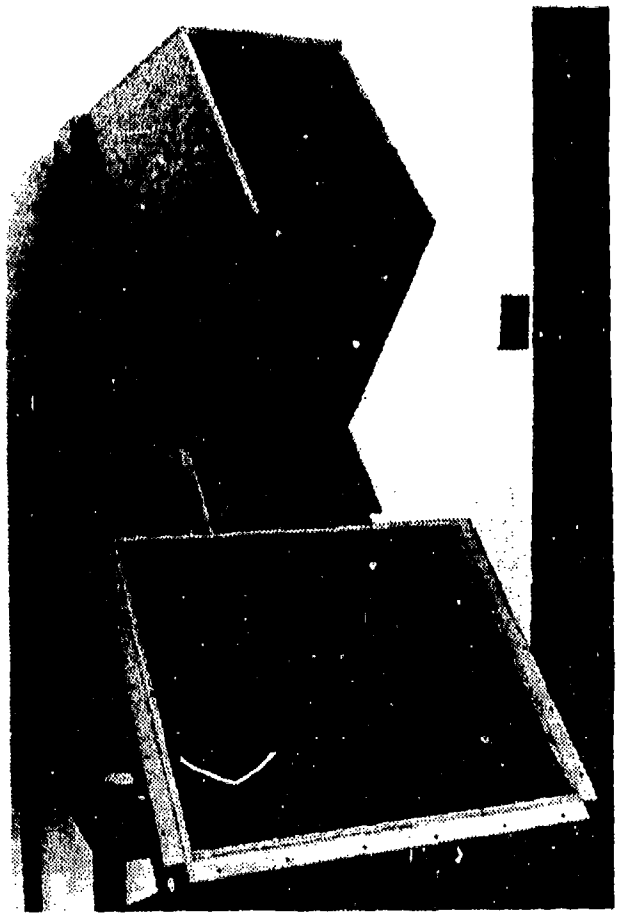

Figure IV-3. Fairing Duct Assembly and Plenum

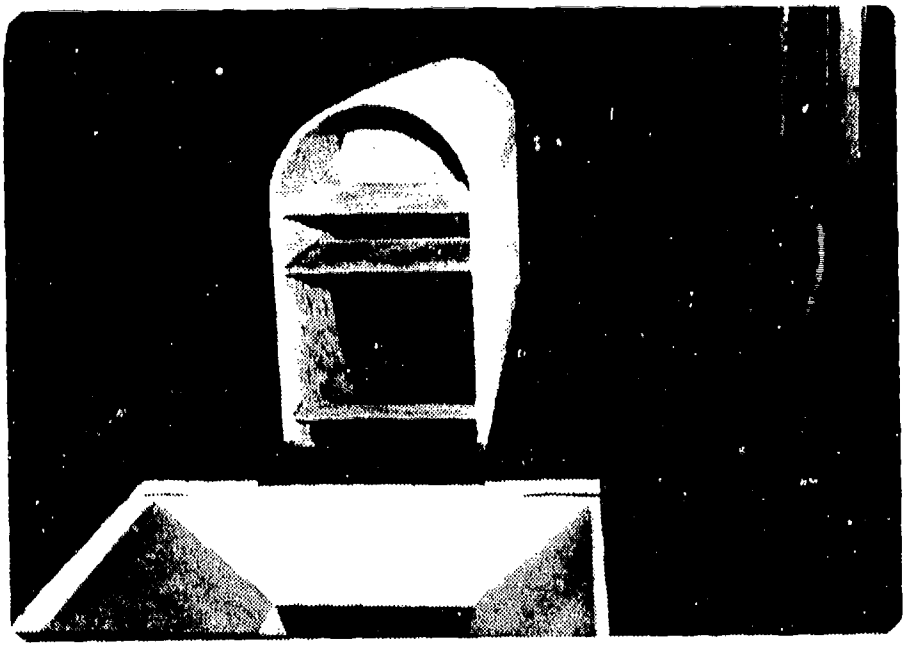

Figure IV-4. Fairing Duct Assembly and Plenum (Installed)

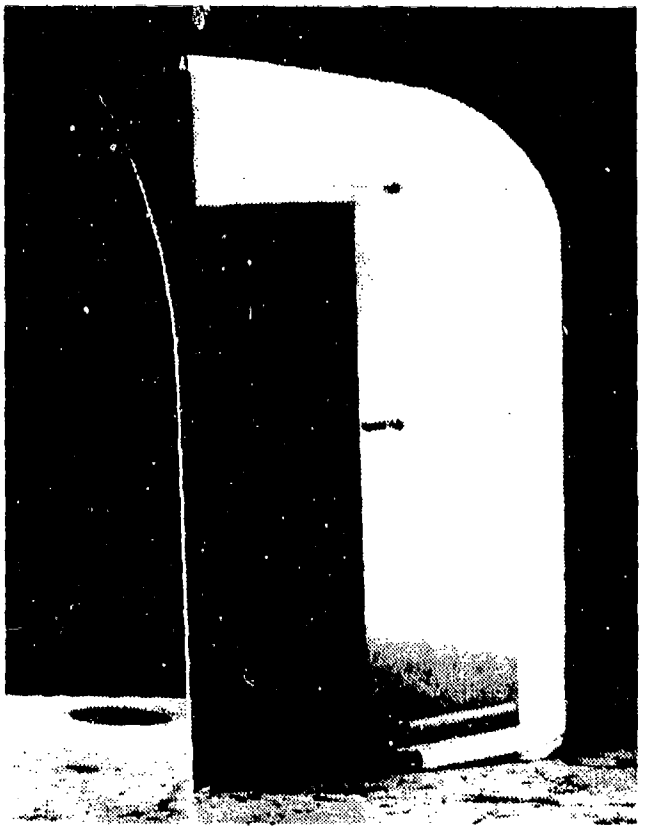

Figure IV-5. Fairing Nose Piece

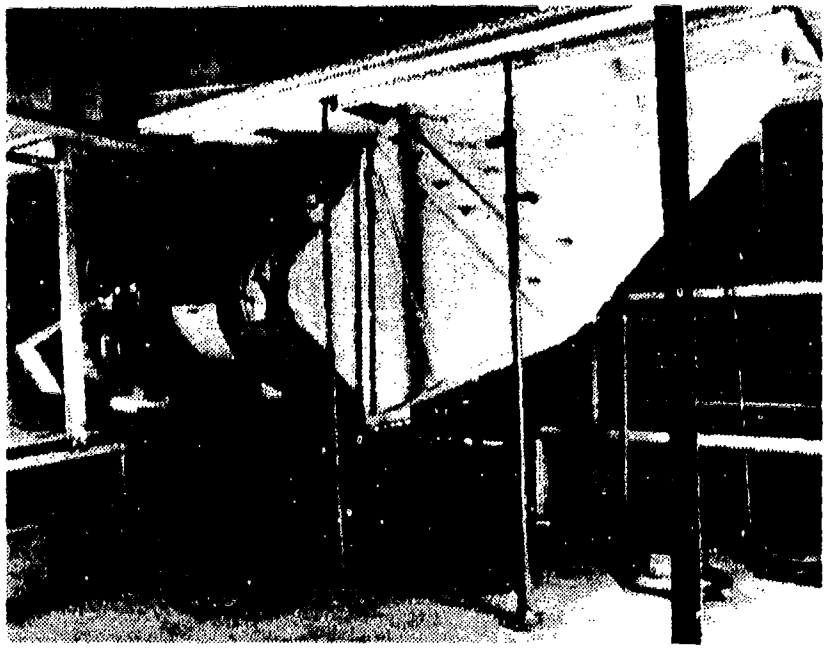

Figure IV-6. Under-Tunnel Assembly (Right Side)

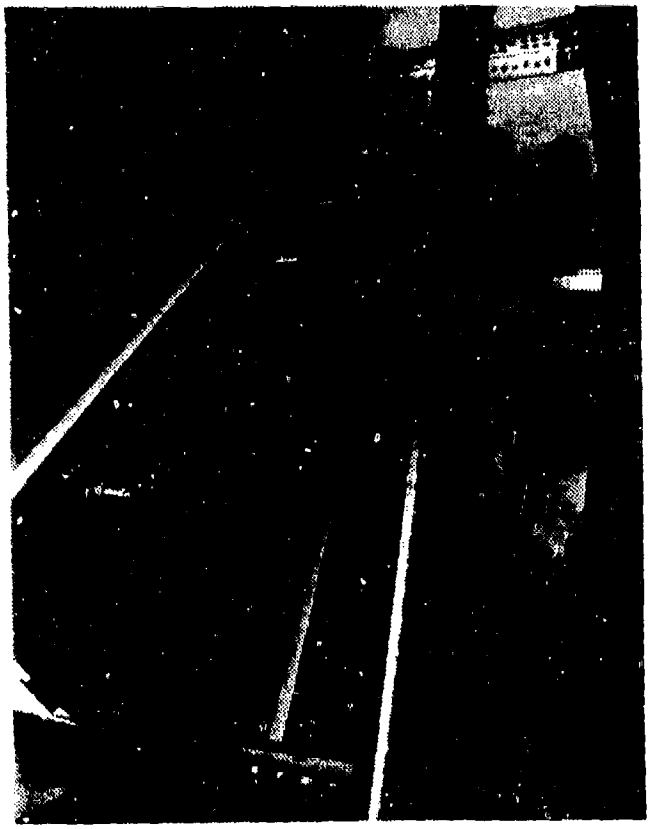

Figure IV-7. Under-Tunnel Assembly (Left Side)

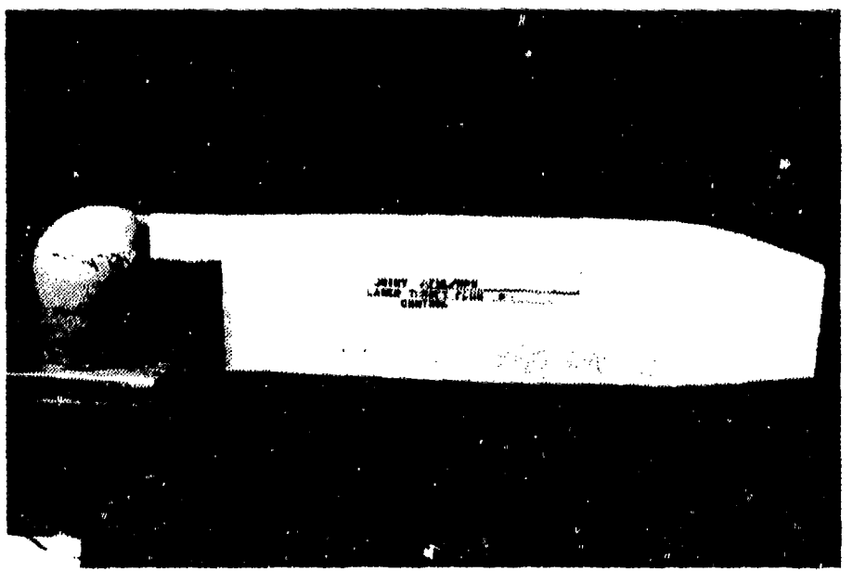

Figure IV-8. Complete Model Assembly in Wind Tunnel (Side View)

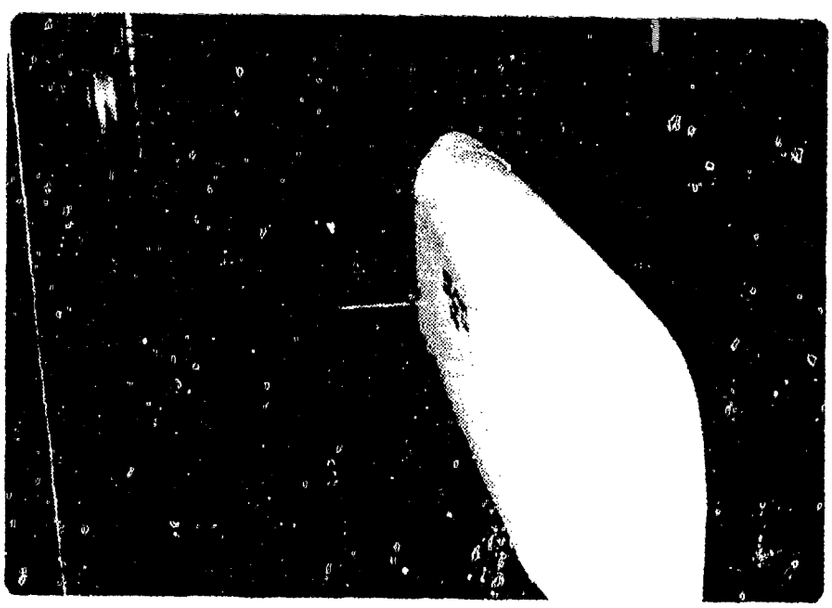

Figure IV-9. Complete Model Assembly in Wind Tunnel (Rear View)

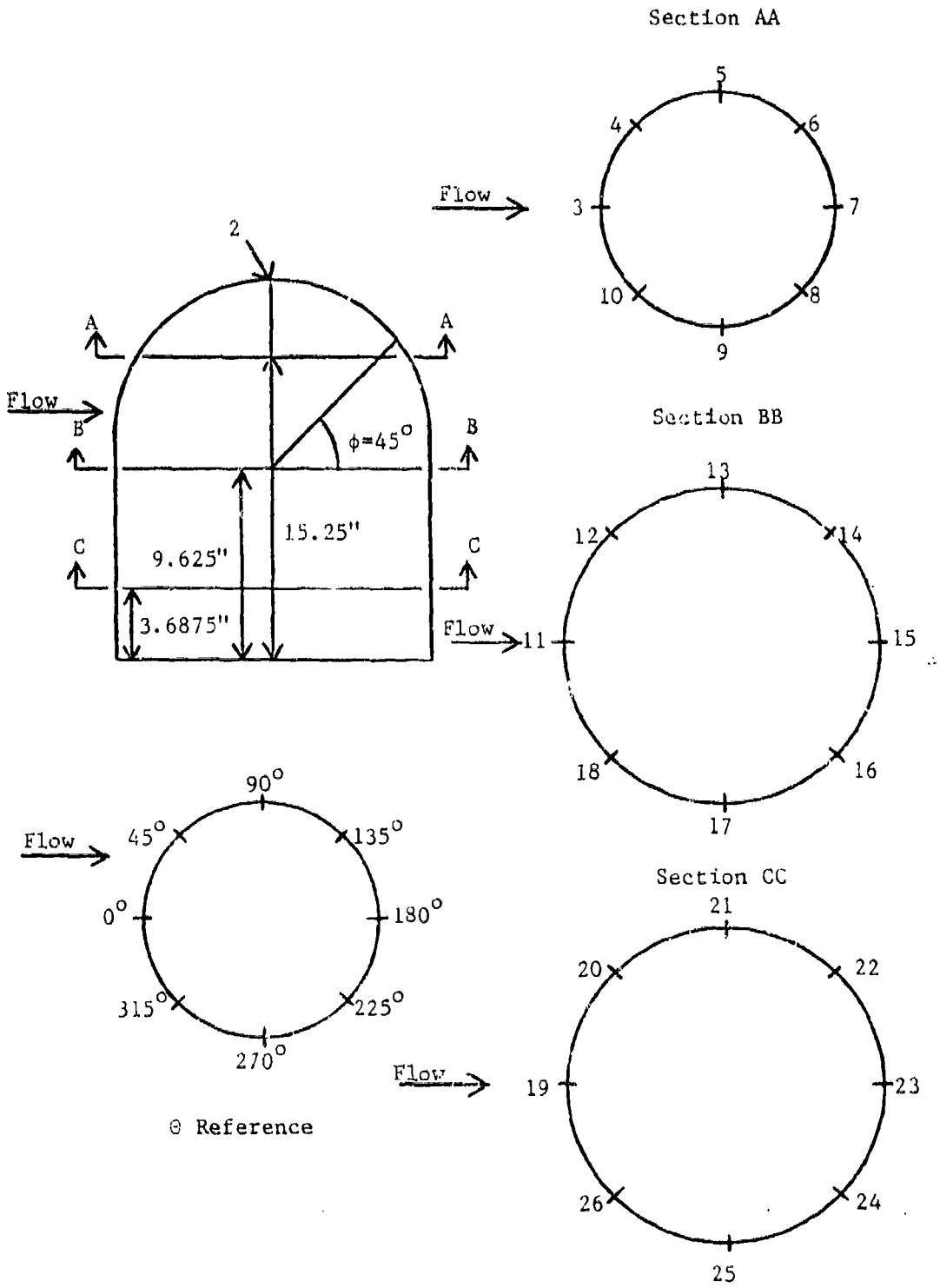

Figure V-1. Turret Pressure Tap Locations

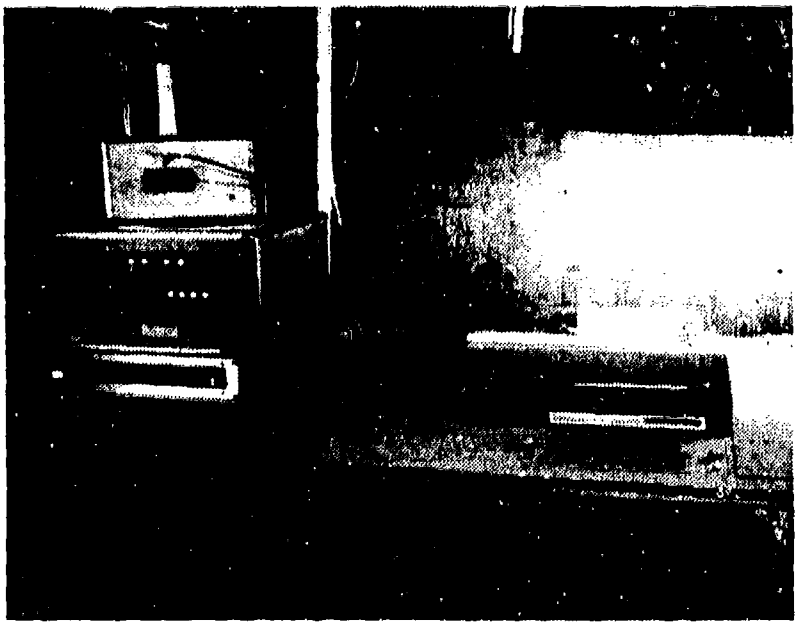

Figure V-2. Wind Tunnel Data Aquisition System

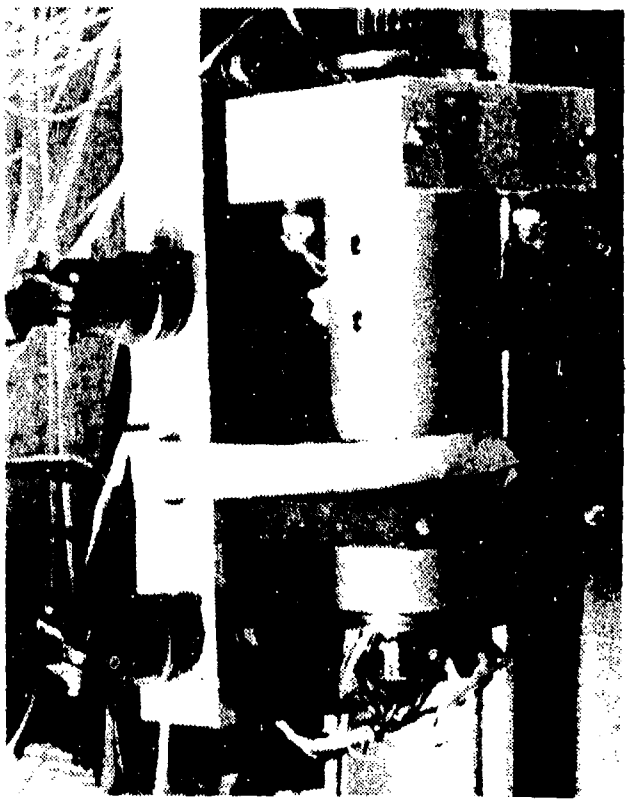

Figure V-3. Scanning Valve

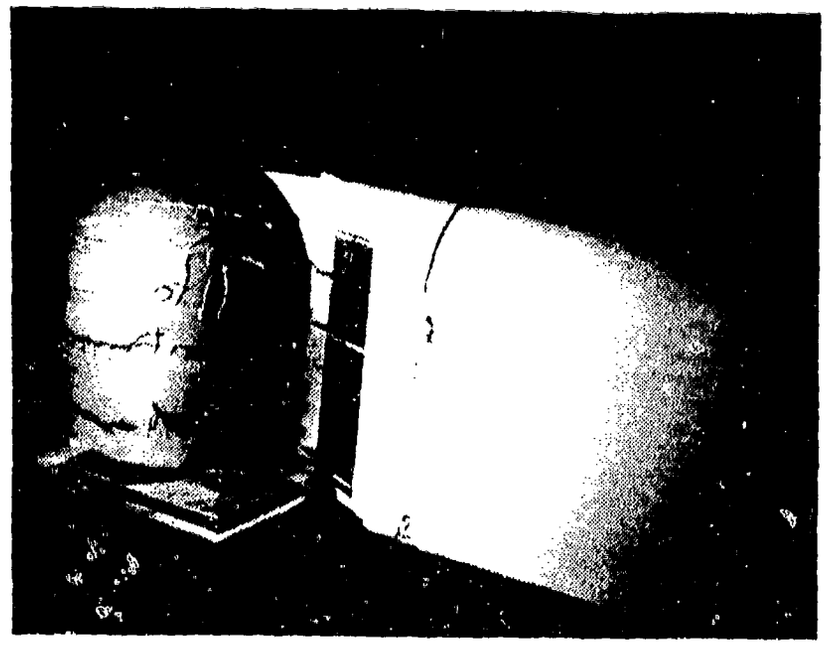

Figure VI-1. Turret without Flow Control Suction

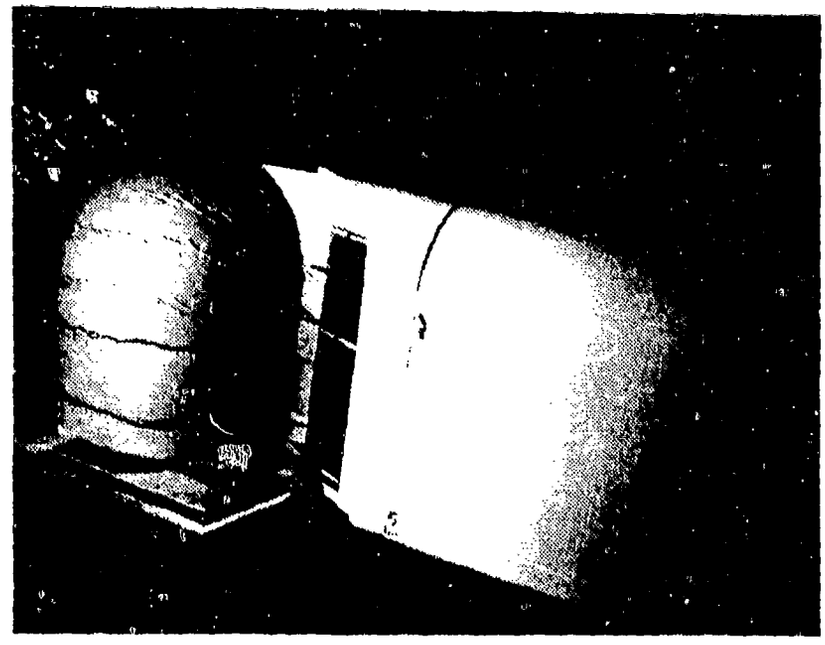

Figure VI-2. Turret with Flow Control Suction

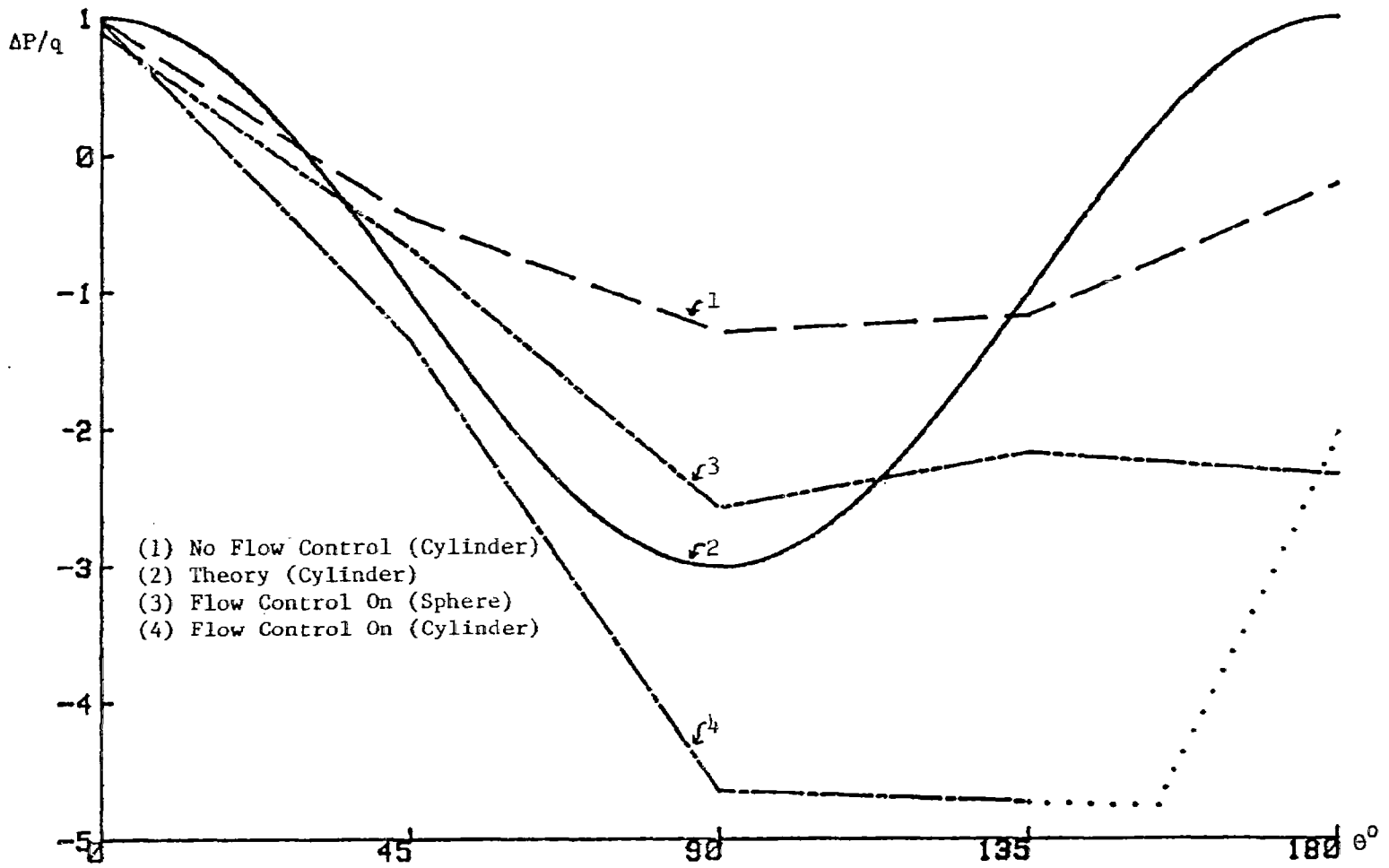

Figure VI-3. Turret Pressure Distribution with and without Flow Control Suction

TABLE V-1

Instrumentation Pressure Tap Location List

Tap #	*Location*	*Tap #*	*Location*	*Tap #*	*Location*
1	Ambient Pressure	16	Turret Hemisphere $\theta = 225°$, $\phi = 0°$	31	Duct 3 dynamic
2	Turret Hemisphere $\theta = 90°$	17	Turret Hemisphere $\theta = 270°$, $\phi = 0°$	32	Duct 3 static
3	Turret Hemisphere $\theta = 0°$, $\phi = 45°$	18	Turret Hemisphere $\theta = 315°$, $\phi = 0°$	33	Duct 4 dynamic
4	Turret Hemisphere $\theta = 45°$, $\phi = 45°$	19	Cylinder $\theta = 0°$	34	Duct 4 static
5	Turret Hemisphere $\theta = 90°$, $\phi = 45°$	20	Cylinder $\theta = 45°$	35	Duct 5 (bottom) dynamic Fuselage boundary layer suction
6	Turret Hemisphere $\theta = 135°$, $\phi = 45°$	21	Cylinder $\theta = 90°$	36	Duct 5 (bottom) static Fuselage boundary layer suction
7	Turret Hemisphere $\theta = 180°$, $\phi = 45°$	22	Cylinder $\theta = 135°$	37	Tunnel Wall 1 (front)
8	Turret Hemisphere $\theta = 225°$, $\phi = 45°$	23	Cylinder $\theta = 180°$	38	Tunnel Wall 2
9	Turret Hemisphere $\theta = 270°$, $\phi = 45°$	24	Cylinder $\theta = 225°$	39	Tunnel Wall 3
10	Turret Hemisphere $\theta = 315°$, $\phi = 45°$	25	Cylinder $\theta = 270°$	40	Tunnel Wall 4
11	Turret Hemisphere $\theta = 0°$, $\phi = 0°$	26	Cylinder $\theta = 315°$	41	Tunnel Wall 5
12	Turret Hemisphere $\theta = 45°$, $\phi = 0°$	27	Duct 1 (top) dynamic	42	Tunnel Wall 6 (rear)
13	Turret Hemisphere $\theta = 90°$, $\phi = 0°$	28	Duct 1 (top) static	43	Impact probe
14	Turret Hemisphere $\theta = 135°$, $\phi = 0°$	29	Duct 2 dynamic		
15	Turret Hemisphere $\theta = 180°$, $\phi = 0°$	30	Duct 2 static		

TABLE VI-1

Estimated Q_r and ΔP_r for Full-Scale Application at Various Altitudes

Alt (ft)	P (atm)	a_∞ (ft/sec)	M_∞	ΔP_r (atm)	Q_r (ft^3/min)
0	1	1116.43	0.5	0.25	612750
10,000	0.6878	1077.39	0.5	0.17	591400
20,000	0.4599	1036.94	0.5	0.11	569200
30,000	0.2978	994.85	0.5	0.07	546100

APPENDIX A

CALCULATION OF VELOCITIES

The calibration procedure determined that $y = 9.2608x + 0.0269$, where y is the pressure in centimeters of water and x is the Scanivalve output value. The pressure was converted from centimeters of water to inches of water as follows:

(y centimeters of water)$\cdot$(0.3937 inches/centimeter) = y inches of water. By the use of a conversion equation, the pressure in inches of water was converted to velocity, measured in feet per second, by means of the following procedure:

$$(y \text{ inches of water})^{\frac{1}{2}} \cdot (4{,}006) = z \text{ ft/min}$$

$$\frac{z \text{ ft/min}}{60 \text{ sec/min}} = z \text{ ft/sec}$$

APPENDIX B

EVALUATION OF THE PRESSURE COEFFICIENT

The pressure coefficient, as given in Eq. 2-7, is:

$$\text{pressure coefficient} = \frac{\Delta P}{q} = \frac{P_s - P_\infty}{q} \quad , \qquad \text{(B-1)}$$

where P_s is the static pressure at the point of interest, P_∞ is the static pressure in the wind tunnel, and $q = P_d - P_\infty$ is free-stream dynamic pressure, the difference between wind tunnel total pressure (P_d) and wind tunnel static pressure. Substituting for q yields:

$$\text{pressure coefficient} = \frac{\Delta P}{q} = \frac{P_s - P_\infty}{P_d - P_\infty} \quad . \qquad \text{(B-2)}$$

Since the calibration equation used in converting the Scanivalve output value for each term in the equation is linear, the calibration factor can be factored and cancelled. Eq. B-2 is used to obtain the pressure coefficient by using only the Scanivalve output values.

APPENDIX C

TEST PROCEDURES SEQUENCE

A. SEQUENCE RATIONALE

The design of the experimental apparatus allowed considerable flexibility in the variation of geometry (turret position relative to the fairing inlet), total suction employed, relative fairing suction rates, and fuselage boundary layer suction rates. The following test sequence was utilized as a step-by-step method to determine the combination of test parameters which provide steady flow with minimum suction--i.e., optimum conditions. Individual tests are referenced to the sequence heading notation corresponding to the particular test parameters being investigated. For example, Test II.B.1 would be the first test run under sequence IIB (turret position aft, fuselage boundary layer suction employed with variable boundary layer suction area).

B. TEST SEQUENCE

I. Turret position aft, no fuselage boundary layer suction

A. Duct butterfly valves fully open

1. Operate with fairing inlet fully open, and vary total blower suction

2. Operate with fairing inlet one half open, and vary total blower suction

3. Operate with fairing inlet partially open, and vary total blower suction

4. Select optimum inlet opening and total blower suction

B. Duct butterfly valves variable

1. Utilize the results of Test I.A.4; vary individual duct suction rates

2. Select the optimum combination

II. Turret position aft, fuselage boundary layer suction employed

A. Utilize results of Test I.B.2; fuselage boundary layer suction inlet fully open, variable boundary layer suction rate

B. Vary fuselage boundary layer suction inlet area, select optimum combination

III. Turret position 4 inches forward, no fuselage boundary layer suction

A. Same sequence as IA series

B. Same sequence as IB series

IV. Turret position 4 inches forward, fuselage boundary layer suction employed

A. Same sequence as IIA series

B. Same sequence as IIB series

APPENDIX D

SELECTED TEST DATA

Included in this appendix are raw test data from two tests. The first set of test data, appearing in Table D-1, is data obtained for turbulent flow about the turret model with flow control suction off. The second set of data, appearing in Table D-2, is data from Test II.B.1 (steady flow with control suction employed). Pressure coefficients, $\Delta P/q$, are listed for all 25 turret pressure ports. Table V-1 gives the locations of the numbered taps.

Table D-1

Test Data with Flow Control Off (Turbulent Flow)

Pressure Tap #	*Scanivalve output*	$\Delta P/q$	*Pressure Tap #*	*Scanivalve output*	$\Delta P/q$
1	0.000	--	25	-0.152	-1.29
2	-0.170	-1.57	26	-0.100	-0.46
3	-0.100	-0.46	27	-0.009	--
4	-0.139	-1.08	28	-0.011	--
5	-0.172	-1.60	29	-0.011	--
6	-0.105	-0.54	30	-0.012	--
7	-0.071	0.00	31	-0.012	--
8	-0.110	-0.62	32	-0.023	--
9	-0.175	-1.65	33	-0.017	--
10	-0.140	-1.10	34	-0.017	--
11	-0.014	0.90	35	-0.073	--
12	-0.104	-0.52	36	-0.069	--
13	-0.172	-1.60	37	-0.024	--
14	-0.099	-0.44	38	-0.071	--
15	-0.071	0.00	39	-0.029	--
16	-0.107	-0.57	40	-0.041	--
17	-0.175	-1.65	41	-0.028	--
18	-0.102	-0.49	42	-0.065	--
19	-0.009	0.98	43	-0.008	--
20	-0.106	-0.56	44	-0.003	--
21	-0.152	-1.29	45	-0.004	--
22	-0.143	-1.14	46	-0.003	--
23	-0.084	-0.21	47	-0.002	--
24	-0.145	-1.17	48	-0.005	--

Table D-2

Test Data with Flow Control On (Steady Flow)
Test II.B.1

Pressure Tap #	*Scanivalve output*	$\Delta P/q$	*Pressure Tap #*	*Scanivalve output*	$\Delta P/q$
1	0.000	--	25	-0.363	-4.65
2	-0.230	-2.54	26	-0.155	-1.35
3	-0.113	-0.68	27	-3.574	--
4	-0.169	-1.57	28	-3.555	--
5	-0.237	-2.65	29	-3.618	--
6	-0.211	-2.24	30	-3.598	--
7	-0.207	-2.17	31	-3.865	--
8	-0.221	-2.40	32	-3.826	--
9	-0.242	-2.73	33	-3.448	--
10	-0.175	-1.67	34	-3.359	--
11	-0.014	0.89	35	-3.353	--
12	-0.136	-1.05	36	-3 333	--
13	-0.291	-3.51	37	-0.026	--
14	-0.246	-2.79	38	-0.070	--
15	-0.217	-2.33	39	-0.024	--
16	-0.253	-2.90	40	-0.039	--
17	-0.295	-3.57	41	-0.026	--
18	-0.143	-1.16	42	-0.061	--
19	-0.009	0.97	43	-0.007	--
20	-0.155	-1.35	44	0.000	--
21	-0.363	-4.65	45	-0.002	--
22	-0.354	-4.51	46	0.000	--
23	-0.195	-1.98	47	0.000	--
24	-0.368	-4.73	48	-0.001	--

LIST OF REFERENCES

1. Mandigo, Alan, *Control of Airflow about a High Energy Laser Turret*, M.S. Thesis, Naval Postgraduate School, 1980

2. Schlichting, Hermann, *Boundary Layer Theory*, 6th Edition, McGraw-Hill, 1968

3. deJonckheere, Richard, *Control of Turbulent, Separated Airflow About Aircraft Turrets*, workshop notes from the Air Force Weapons Laboratory Workshop, Albuquerque, NM, 10-11 March 1980

4. *U. S. Standard Atmosphere, 1976*, National Oceanic and Atmospheric Administration, National Aeronautics and Space Administration, United States Air Force, U. S. Government Printing Office, 1976

5. Liepmann, H. W., and Roshko, A., *Elements of Gas Dynamics*, Wiley & Co., 1957

A silent 16-mm movie, seven minutes in duration, is available on loan to interested parties. The movie shows turret tuft motion with and without flow control employed. Requests should be directed to Professor Allen E. Fuhs, Code 67Fu, Department of Aeronautics, United States Naval Postgraduate School, Monterey, California 93940. Telephone: Commercial, (408)-646-2948, or AUTOVON, 878-2948.

INITIAL DISTRIBUTION LIST

	No. copies
1. Defense Technical Information Center Cameron Station Alexandria, Virginia 22314	2
2. Library, Code 0142 Naval Postgraduate School Monterey, California 93940	2
3. Department Chairman, Code 67 Department of Aeronautics Naval Postgraduate School Monterey, California 93940	1
4. Professor Allen E. Fuhs, Code 67Fu Department of Aeronautics Naval Postgraduate School Monterey, California 93940	10
5. Lt. James Schonberger, USN 1920 Catherine Drive Bismarck, North Dakota 58501	2
6. Captain Richard deJonckheere, USAF AFWL, ARLB Kirtland Air Force Base Albuquerque, New Mexico 87177	10
7. Lt. Alan M. Mandigo, USN 208 Dunning Drive Camillus, New York 13031	2